Sensors & Actuators: B. Chemical 395 (2023) 134441

Contents lists available at ScienceDirect

Sensors and Actuators: B. Chemical

journal homepage: www.elsevier.com/locate/snb

Dual-valved skin-interfaced microfluidic device for programmed time-control sweat collection

Ji Hyun Yang [a], Uchekuwu David [b], Yeon Sik Noh [b], Ahyeon Koh [a,*]

[a] Department of Biomedical Engineering, State University of New York at Binghamton, Binghamton, NY 13902, USA
[b] College of Nursing and Department of Electrical and Computer Engineering, University of Massachusetts, Amherst, MA 01003, USA

ARTICLE INFO

Keywords:
Soft microfluidic valve
Sweats sensing
Dual valve
Thermal expansion valve
Capillary burst valve

ABSTRACT

Biomarkers in human sweat can provide valuable insights into physiological states, identify diseases, and help clinicians understand patients without invasive measurements. However, obtaining accurate long-term data from sweat using current sweat collection methodology raises doubts. Here, we describe a soft-bioelectronic platform that uses a thermal expansion valve to collect sweat under programmed time control. By incorporating expandable microspheres, the skin-interfaced microfluidic device platform merges capillary burst valves and irreversible-thermal expansion valves. An expansion layer below the microfluidic channels expands irreversibly upon heat delivery from underlying microheaters. The thermal expansion valve isolates the collected sweat into separate chambers to minimize internal mixing. The human study demonstrates that our novel time-programmed sweat collection device improved sweat analyte data (sweat volume, pH, lactate, and cortisol) from the conventional sweat collection. In addition, the human study results indicate a correlation between sweat rate and sweat lactate with aerobic and anaerobic exercises. Our approach can be integrated with past and current microfluidic systems and other chemical sensing modalities, such as colorimetric and electrochemical measurements of sweat analytes present in current sweat devices for advanced on-board diagnostics.

1. Introduction

Skin-interfaced, wearable microfluidic devices, also called epifluidic, provides a platform for sweat collection and evaluation, allowing non-invasive investigation of human physiology in real time [1–11]. Sweat biomarkers found in sweat are similar in the blood, ranging from ions, molecules, amino acids, exogenous drugs, and small proteins but not in the concentrations. Information about chloride in the sweat is a gold standard for diagnosing cystic fibrosis [12], and sweat glucose analysis has been highlighted for potential diabetes management [13]. Other physiological biomarkers, such as ethanol, lactate, and cortisol, can reveal information such as alcohol levels, muscle fatigue, and stress levels, respectively [14]. Trace amounts of sweat analytes exist in sweat and can be analyzed through in situ, on-board analytical instrumentation using electrochemical and spectrometric systems. Notably, a skin-interfaced 3D microchannel allows accurate, quantitative sweat analysis without concern about solvent evaporation during the biosensing and sampling.

Despite advances in material design and microfluidic analytics for sweat monitoring technologies, there is still a lack of complete understanding regarding the time-dynamic response of sweat physiology and the involvement of sweat biomarkers. This is primarily due to the vast complexity of the transportation of analytes from blood to sweat compounded by human physiological processes. Additionally, sweat analyte exhibits different transportation mechanisms from the blood to sweat depending on the size, chemical, and biological characteristics. Spatiotemporal analysis of on-body sweat could demonstrate reliable information to determine abnormalities in the sweat analyte concentrations, even in trace amounts, for further clinical testing using standard blood measurement [15,16].

Developing soft-elastomeric material for epifluidics realizes wearable systems that directly collect sweat in microfluidic channels and chambers through secretion pressure and capillary action. The soft wearable systems can be mounted on nearly every body part with sweat glands, allowing continuous access. The design of epifluidic devices must consider parameters such as channel dimensions and chamber capacity based on various factors, including perspiration characteristics (total of 0.5 – 2 Lh^{-1} during physical exercise from the whole body) [17,18]. Other factors include the body location, the size of the device, on-board measurement capabilities, the number of analyses, and the

* Corresponding author.
E-mail address: akoh@binghamton.edu (A. Koh).

https://doi.org/10.1016/j.snb.2023.134441
Received 13 June 2023; Received in revised form 28 July 2023; Accepted 10 August 2023
Available online 14 August 2023

lifetime of the sensing system. The epifluidic platform provides a home for integrating analytical instrumentation, such as flexible electrochemical sensors, graphene-based field effect transistors, aptamer biosensors, and colorimetric responsive materials [3, 19–28]. Additionally, the epifluidic device holds the potential to integrate valves, pumps, and multiplexers to manipulate the collection and storage of biofluids and enhance sensor performance [29–35]. The advances in skin-interfaced microfluidics have revolutionized various applications, enabling remarkable achievements such as underwater detection [36] and energy harvesting and production [37–39], ushering in a new era of versatile and integrated wearable technologies.

Recently reported skin-interfaced sweat devices can detect metabolites in sweat at acceptable accuracies, such as sodium [17,40], glucose [31,41], and lactate [42,43], because of their large abundance compared with other sweat analytes. Further in-depth analysis of trace analytes (e.g., proteins and steroids) may require offline measurements through the extraction of the fluid from the sweat collection platform and delivered to sophisticated laboratory instruments that possess greater precision and accuracy [44–46]. However, most sweat collection devices accumulate sweat in the same chamber without considering the temporal information for quantitative analysis [47]. Such collection approach fails to reflect the dynamic concentration fluctuation. Therefore, separating sweat in each chamber to each physiological event is crucial to enhance our understanding of sweat physiology further. For example, sweat analysis for circadian secreted biomarker detection (e.g., cortisol) highly relies on exclusively controlled in situ chronosampling [20,48]. Indeed, a reform in the sweat collection is necessary to comprehensively understand the time-dependence aspect of sweat analyte composition and its relationship with human physiology; thus, the sweat collected at improved temporal resolution can be analyzed for on-board and offline measurements [49,50].

The recent state-of-art in epifluidics has achieved sweat chronosampling. Passive capillary burst valves (CBV) were integrated into the soft microfluidic channel design for the sequential sweat collection in separate chambers while assuming a constant flow of sweat [34]. Another approach to sweat sampling used hydrophobic valves and superabsorbent polymers (SAP) for the sequential collection of sweat by closing the channel pathway through the expansion of the SAP in the channel after filling the chamber, which manages the direction of the sweat flow [33]. However, similar to CBV, the sequentially collected sweat is limited by absolute time information unless all the chambers were filled at a constant flow rate allowing for controlled estimation. Furthermore, galvanic stopwatch sweat devices have been developed using galvanic cells to register time stamps to overcome limitations [51]. Each galvanic cell is embedded at an individual microfluidic chamber's entrance and activated upon sweat fluid entry. Despite simultaneously generating electronic signals to write the time of sweat entry, sample mixing in the chamber needs to be solved. The most recently developed time-dependent epifluidics use hydrogel-based microelectronics for a wearable valving system along with electronics [35]. The electronics allow a smartphone application to deliver localized heat on-demand to change the volume of the hydrogel at the outlet, relieving back pressure for fluid entry into each compartment. However, the device requires continuous power consumption during the sweat collection to maintain the open gate status of the chambers. Additionally, it may not be possible to achieve segregation of sweat collection if the hydrogel valve is located at the end of the chamber. Consequently, there is a possibility of potential mixing occurring at the device inlet due to human movement or natural molecular diffusion. This is due to the location of the hydrogel valve, where absorption and desorption of the hydrogel (valve actuation) could potentially interfere with the sweat measurement technology.

This article presents a dual valve-controlled skin-interfaced microfluidic system for time-dependent sweat collection using a programable FHE system. The epifluidics comprise a thermal expansion valve (TEV) that effectively closes the channel at the chamber entrance based on a microcontroller in the flexible hybrid electronics (FHE) and a CBV for chronological fluid filling. The instant TEV activation blocks the microfluidic pathway and reduces molecular diffusion, minimizing sample contamination regardless of sweat flow characteristics in the device. The TEV is composed of heat-expandable microspheres and polydimethylsiloxane (PDMS). The valve expands under heat in the microfluidic channel space and closes the channel at the chamber entrance based on a microcontroller in the FHE. The instant TEV activation blocks the microfluidic pathway and reduces molecular diffusion, minimizing sample contamination regardless of sweat flow characteristics in the device. The exquisitely designed dual-valved epifluidics ensure sweat harvesting on a computed time frame under extreme mechanical distortion. The fabricated device characteristics appeal to encounters in sports, military, medical, and related applications that require offline measurement of sweat analytes for high precision.

2. Results and discussion

2.1. Device characteristics and operational principles of the time-controlled sweat sampling microfluidics

Fig. 1A illustrates the fabrication of the skin-interfaced soft microfluidic device for time-controlled sweat collection. Soft lithography of PDMS allows the creation of microfluidic channels, chambers, and valves enclosed with an elastomeric layer through oxygen plasma bonding. The natural hydrophobicity of PDMS may have an impact on device performance, particularly concerning long term sample storage and analytics due to biomolecule adsorption and sample evaporation [52–54]. While the comparison of devices will focus on sweat sampling and analysis, fabrication material remains a crucial factor in the future development of microfluidic devices. Optimizing sample storage capabilities and considering the analytical implications of the fabrication material will be of utmost importance in this regard.

The fabricated device features six chambers, each with a capacity of approximately 23 μL, specifically designed to collect human sweat throughout the day with programmed collection times facilitated by the flexible hybrid electronics (FHE). Once collected, the sweat can be analyzed using laboratory instrumentation after removal from the skin. The chambers are designed in a serpentine manner (width: 2000 μm, height: 200 μm) to ensure structural integrity even under mechanical distortion and to prevent the formation of air pockets, thereby allowing each chamber to be filled completely [55,56]. Given the substantial volume of sweat that can be collected in each chamber compared to other devices in the literature (**SI Table 1**), careful optimization is required for integrating real-time sensing modalities for future on-board electrochemical or colorimetric applications to ensure accuracy and precision. The generous capacity of the chambers makes this device particularly valuable for users in environments with extensive sweat production, such as athletes and workers in extreme conditions (e.g., firefighters).

Each chamber ends with a circular chamber (dia. 750 μm) that can be incised to allow micropipette access for fluid collection. The transfer-printed microheater on the expandable layer is connected to the FHE through an FPC/FFC (Flexible Printed Circuit/Flexible Flat Cable) that provides programmable power delivery to a microheater. The off-the-shelf FPC/FFC connection provides an easy connection of the skin-interfaced microfluidics to electrical circuitry that can be potentially used for electrochemical analysis. In addition, the separating electrical components to FHE and microfluidic device solely for collection allows the used microfluidic device to be replaced with a new device to collect extra sweat, demonstrating disposable and reusable characteristics.

The dual-valve system consists of CBV and TEV to achieve an exquisitely time-controlled sweat collection aided by FHE. The CBVs direct the flow sequentially based on the liquid pinning at the diverging section of the channels with the fluid introduction (Fig. 1B a-c) [34]. When the sweat rate is inconsistent or periodic, a sweat sample collected

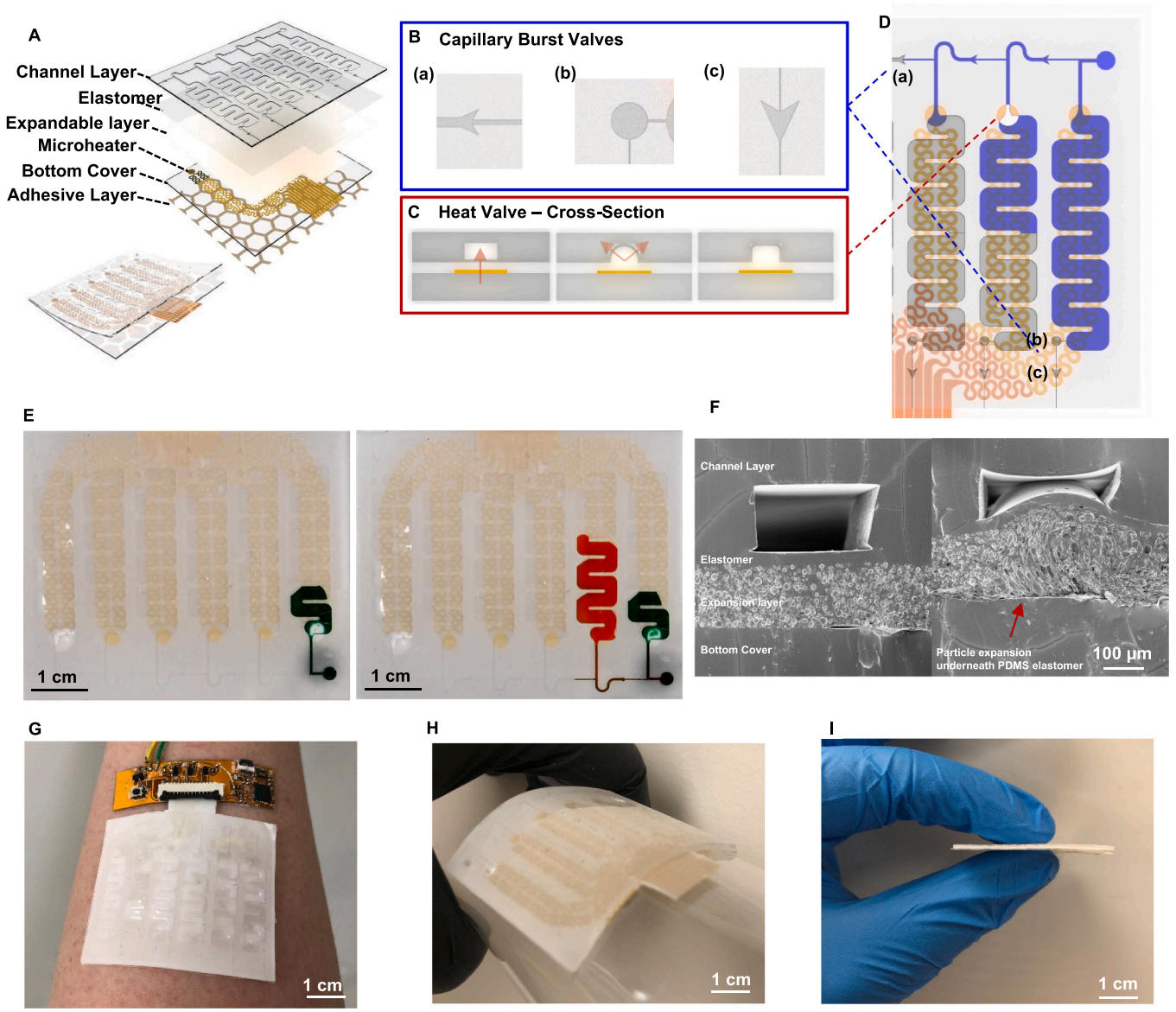

Fig. 1. Design features and operating characteristics of a skin-interfaced microfluidic device for sweat collection and analysis. A. exploded view of the microfluidic device set-up for sweat collection. B. Close-up view of the key CBVs integrated in the microfluidic channels in the device for chronological collection. C. simple block diagram showing the progression of the TEV in the microfluidic device channels after activation. D. Image of a microfluidic device filling scenario with fluid with after interaction using CBV and TEV. E. Photograph of working microfluidic device filled with colored solution, green then red, after intervening with TEV before fully filled. F. Cross-section scanning electron microscopic image of TEV before and after activation. G. Image of microfluidic device connected with FHE. H. Image of microfluidic device under bending condition, I. Hand-held side-view image of microfluidic device.

in a single chamber can represent multiple sweating events and result in biomarker accumulation and mixing (**SI Video 1**). In addition, sweat rate and volume vary up to 2000 ml/hr from the entire body depending on the activity, location on the body, gender, ethnicity, and genetics as individuals respond differently to physical and chemically-induced stimuli [57,58].

Supplementary material related to this article can be found online at doi:10.1016/j.snb.2023.134441.

To achieve exquisitely time-controlled sweat sampling, TEV is introduced. The TEV can be activated at a programmed time as the microheater causes blocking the fluid by the irreversible expansion of the microspheres (SI Fig. 1). The high channel blockage because of the channel closure detours the fluids to the next chamber on demand, similar to CBV mechanism for flow control (Fig. 1C). Scanning electron microscope (SEM) images (Fig. 1F) indicate that activation of the TEV valve at the chamber entry with ~95% volume closure, significantly increasing the flow blockage of the channel. Dual-valve characteristics enable on-demand, precisely controlled sequential sweat collection for time-dependent biochemical analysis by combining passive CBV and active TEV valves (Fig. 1D-E). The fabricated sweat collection device (Fig. 1G-I) comprises PDMS, a silicone elastomer exhibiting similar skin mechanics. The microfluidic device weighs ~2.6 g and measures 42 × 50 × 0.7 mm. The dimensions allow microfluidic device installation on various human skin surfaces, including the forearm, chest, and lower back, where the most eccrine sweat glands are available for sweat collection. A double-sided thin adhesive (0.85 MPa of adhesion force) and the thin architecture of the device facilitate conformal attachment to the skin and minimal delamination.

2.2. Operating characteristics of TEV and embedded microheaters

TEV valves have two main components: an expandable layer for

thermal expansion under heat and a microheater for heat delivery. The expandable polymers in the expandable layer require 80 °C to reach the glass transition temperature for the gas trapped in the expandable microsphere to expand in volume irreversibly. Micropatterned gold traces were transfer printed underneath the expandable layer, providing the heat for the expansion process (Fig. 2A). The circular portion of the gold trace operates as a resistor for spatial activation of TEV. At the same time, the ends of serpentine connectors work with the FHE. Upon TEV activation by a current, a brighter white color and the simultaneous bulging of the surface were observed for ~4 s because of the expansion of the microspheres by heat (Fig. 2B). Infrared images in Fig. 2C confirm the temperature increase is restricted to the circular region during TEV activation while there are negligible temperature changes along the serpentine lines (SI Video 2A-C). The circular portion of the microheater is designed with thinner lines (75 μm) compared with the connecting lines to the FHE (150 μm), and the meandering structure ensures significant temperature increments compared to the rest of the microheater structure. The proposed microheater activation scheme avoids unwanted thermal expansion along connectors as it fails to reach the activation temperature of the expandable microspheres (~80 ℃).

Supplementary material related to this article can be found online at doi:10.1016/j.snb.2023.134441.

The temperature profile at each resistor for TEV activation is described in Fig. 2D. The microheaters reach the activation temperature within ~5 s of power delivery. The temperature increments of the microheater differ depending on its location, as the length of connecting lines to the FHE changes the total resistance of each microheater. In the middle and outermost microheaters, activation time increases by 16% and 35%, respectively, compared with the inner microheater. However, the difference in the temperature profiles of the inner, middle, and outer microheaters can be minimized by adjusting the electric current and voltage delivered from the FHE. Reducing the thermal-based

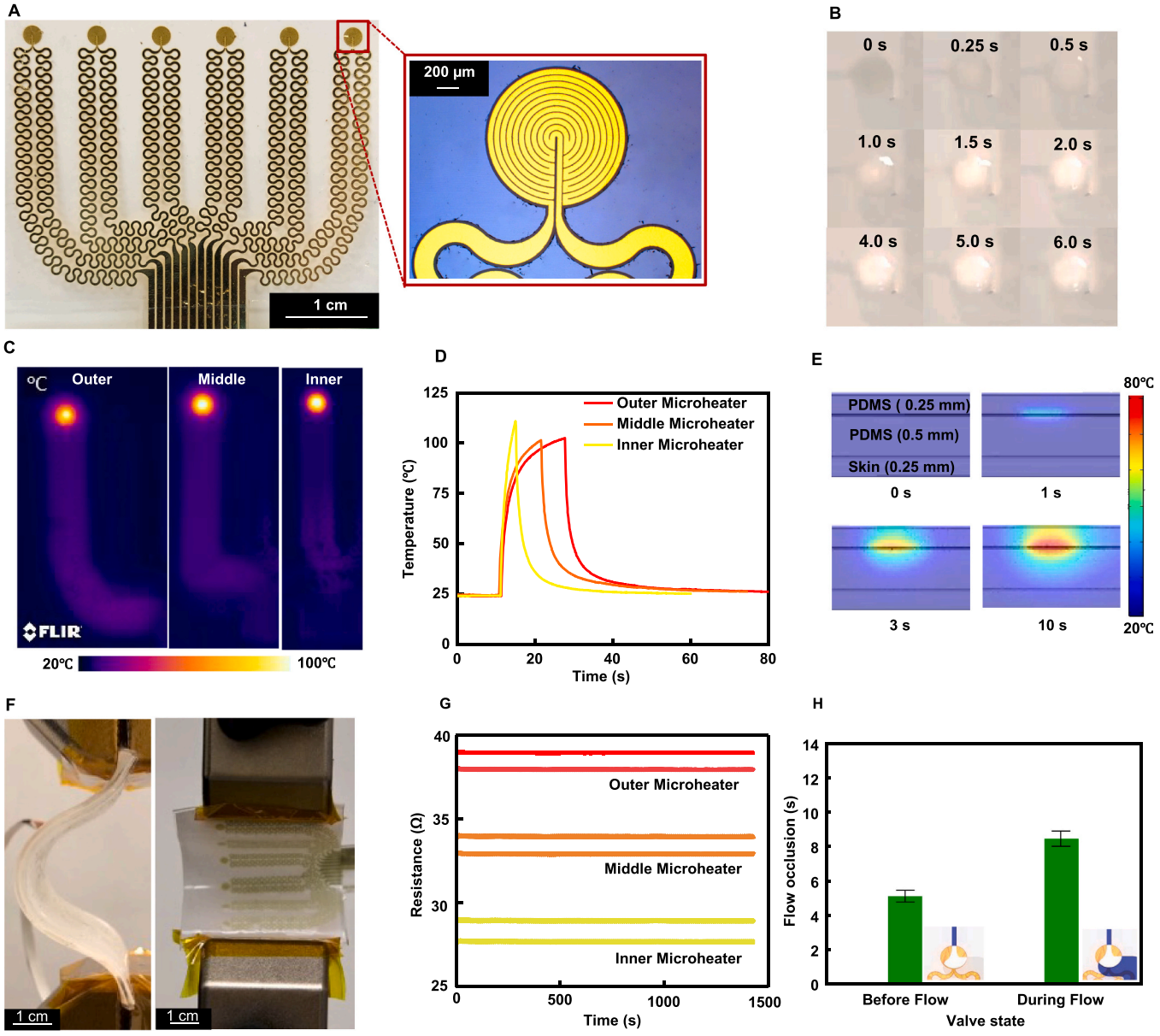

Fig. 2. Microfluidic device characterization. A. Image of the microfluidic device and its microfluidic flow pathway without thermal valve intervention. B. microfluidic CBV characterization using SEM images. C. Burst pressure characterization of the CBV and TEV. D. Microfluidic device filling time under constant pressurized flow condition. E. Microfluidic device filling time under discontinuous and burst pressure filling condition. F. Image of microfluidic under mechanical bending condition with fully filled solution. G. Resistance changes in the microheaters under mechanical bending conditions over time. H. Bar graph describing time required for full activation of the TEV under no flow and flow condition.

microheater activation time is crucial to avoid burning the microfluidic device's user. The irreversible expansion is ideal for skin-interfaced microfluidic device applications because it does not require additional energy to keep the channel closed completely. The simulation estimates the microheaters' thermal conduction and temperature profile on the human skin during activation (Fig. 2E and SI Video 3). The temperature profile against time shows that significant heat does not reach the skin during device activation. Therfore, TEV activation will not cause heat-induced sweating as it involves instantaneous and localized heating with a polymeric barrier that minimizes changes in skin temperature. While the TEV requires 80 °C for activation, the rapid activation time, localized heating, and the presence of thermal barriers (such as PDMS and medical adhesive) can effectively mitigate the risk of thermal damage to the skin tissue. The microheater lines to the FHE connectors are designed as serpentine structures to also provide flexibility and stretchability under the natural movement of the human skin. The resistance of the microheaters was measured under mechanical cycling bending conditions (SI Video 4), and the results showed minimal effect on the resistances of the microheaters after 1000 cycles of repeated mechanical bending (Fig. 2F and G). The channel's microheater activation time with and without microfluidic flow was evaluated to define the maximum activation time. The activation time was based on the outermost microheater. The TEV activated and fully closed the channel in 4 s without the liquid flow and 10 s with the liquid flow (Fig. 2H). Pre-wetting the channel before TEV activation decreases resistance to microfluidic flow and prolongs the time needed for microfluidic flow blockage. The optimized microheater activation scheme achieves safe and reliable operation for TEV-controlled microfluid collection for skin-interfaced application.

Supplementary material related to this article can be found online at doi:10.1016/j.snb.2023.134441.

2.3. Microfluidic device characterization for skin-interfaced application

The skin-interfaced microfluidic device requires hydrodynamic flow robustness for varied secretory fluidic gland pressure. Therefore, numerous in-vitro microfluidic flow experiments were performed at different microfluidic pressures, all within the range of physiological sweat pressure. The designed microfluidic filling profile is outlined in Fig. 3A in the order of I to V. The sequential filling of the microfluid is based on the passive CBV system. The detailed mechanism follows from the Laplace-Young equation below for rectangular channels:

$$Burst \quad Pressure = -2\sigma\left[\frac{\cos\theta_I^*}{b} + \frac{\cos\theta_A}{h}\right],$$

where σ is the surface tension of the liquid, θ_A is the contact angle of the channel, θ_I^* is the min $[\theta_A + \beta;\ 180\ ^\circ]$, β is the diverging angle of the channel, and b and h are the width and the height of the diverging section, respectively [34]. The burst pressure characterization allows the microfluidic flow to fill in the order of low to high burst pressure. Fig. 3B illustrates the detailed dimensions and close-up SEM images of

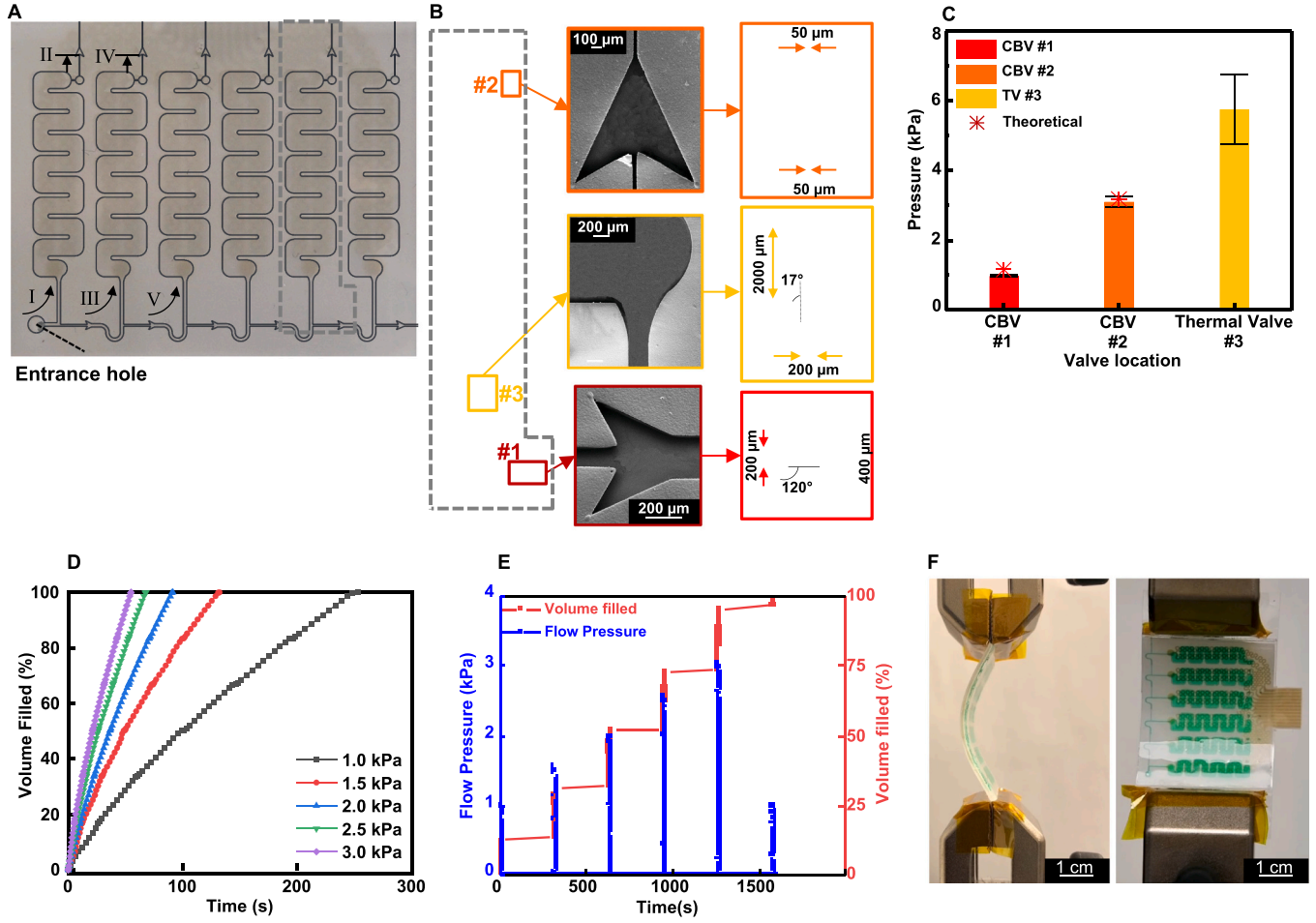

Fig. 3. Microfluidic device characterization. A. Image of the microfluidic device and its microfluidic flow pathway without thermal valve intervention. B. microfluidic CBV characterization using SEM images. C. Burst pressure characterization of the CBV and TEV. D. Microfluidic device filling time under constant pressurized flow condition. E. Microfluidic device filling time under discontinuous and burst pressure filling condition. F. Image of microfluidic under mechanical bending condition with fully filled solution.

the CBV used in the microfluidic device. The CBVs #1 and #2 exhibit a diverging angle of 120 °, channel height of 200 μm, and channel width of 200 μm and 50 μm, respectively. The microfluidic burst pressures were determined for the CBV and TEV system and are shown in Fig. 3C. The burst pressure was recorded by applying a steady increase of pressure increments at the passive valve interface. The result shows that passive valves #1 and #2 have a burst pressure of about 1.0 kPa and 3.0 kPa, respectively. No significant difference was observed between the theoretical and experimental results. The pressure generated by the eccrine sweat glands ranges from 0.5 to 2.5 kPa [59]. Therefore, the CBV design ensures the sequential filling requirement. During the measurement of burst pressure for the TEV, delamination was observed between the channel layer and the elastomeric layer at the TEV location. This delamination occurred due to the significant pressure required to force liquid through the closed channel of the TEV. High pressurized flow can cause such delamination issues. Consequently, the burst pressures for the TEV were also recorded as the pressure at which the delatmination occurred. The TEV exhibited a significantly higher burst pressure (~6 kPa) than the CBV burst pressures, clearly indicating its effective blocking of the flow and successful achievement of the device's intended flow design for programmed time-controlled collection. Thus, once the TEV is activated, the TEV retains the highest burst pressure for flow. The constant pressurized flow in the range of 1.0 kPa to 3.0 Pa displays a stable sequential filling profile despite the integration of CBV in the structures (Fig. 3D). The ~150 μL total capacity is filled in about 1.5 min at 2 kPa constant pressure, that displays an average flowrate of 100 μL min^{-1}. Physiological sweat rates for eccrine sweat glands vary from 12 to 120 μL $hour^{-1}$ cm^{-2} [18]; for a collection area of r = 6 mm, the physiological sweat rate ranges from 13.5 to 135 μL $hour^{-1}$, which satisfies the practical use requirements. Each microfluidic chamber of ~23 μL capacity is designed to contain sweat generated for 15 min–3.5 h. The periodic constant pressurized flow profile was conducted to implement extreme sweating events (Fig. 3E). The periodic filling at different constant pressurized flows did not compromise the sequential filling of the microfluidic device within the physiologically relevant pressure. Simultaneously, the effect of any backpressure was assessed and showed that there were very minimal to no backflows during the rest period. Avoiding backflow is essential in epidermal microfluidic applications to retain the sweat within the device for on-board sensing modalities or storage for laboratory analysis. To test stability in the stored sweat sample, the maximum bending angle was evaluated to find when the microfluidic device started to leak. The maximum bending radius before fluid leakage was determined to be ~20 mm (Fig. 3F and SI Video 5). The measured bending radius can facilitate skin-interfaced attachment at most eccrine sweat gland regions, such as the forearm, chest, lower back, and forehead. Microfluidic design parameters such as channel dimensions and chamber capacity can be modified to a larger or smaller capacity, and the number of chambers can change depending on the application requirement. Each chamber space can be used as an assay zone for an in situ electrochemical and colorimetric detection of desired single or multiple analytes. The current epifluidic device can be used for a sweat-collection platform, and sample extraction capabilities were tested in standard laboratory 200 μL and 1000 μL pipettes (SI Video 6). The small circular incision at the end of the chamber provides access to the pipette tip. The results showed that both pipettes could collect samples close to the theoretical amounts. The slight variance may be caused by the user handling of the pipette controlling the suction pressure, leading to unrecovered samples along the channel corners. The microfluidic assessment of the fabricated device with TEV integration displays robust fluidic characteristics for epifluidic applications.

Supplementary material related to this article can be found online at doi:10.1016/j.snb.2023.134441.

2.4. In vitro microfluidic device testing for TEV-controlled collection

The feasibility of the TEV-integrated microfluidic device was checked with FHE. The experiment was conducted in a laboratory with a benchtop apparatus to resemble skin-interfaced conditions (SI Fig. 2). Fig. 4A demonstrates the working mechanism. The first chamber was filled with green fluid until the TEV actuation interrupted the flow. The filling then continued with a red fluid right after the TEV activation, routed into the second chamber due to TEV (SI Video 7). The result from the dyed solutions coincides with the predicted chronological filling and the burst pressure assessment of the CBV and TEV. Multiple combinations of solutions with different pH levels (pH 1, 7, and 14) were sequentially introduced into six chambers to amplify any internal mixing problem and test for small molecule (i.e., proton) diffusion across the TEV. Different pH solutions also represent sweating events. The microfluidic filling profile using pH solutions was filled without (Fig. 4B) and with (Fig. 4C) TEV activation to separate pH solution to respective chambers. The fluids from the sequential pH filling were collected and measured for pH levels (Fig. 4D). Without TEV activation, the continuously filled device fails to resemble the pH filling pattern due to inevitable mixing in the same chambers. Moreover, the fluid collection process using a pipette is predicted to cause significant mixing before the pH measurement. The dual valve sweat collection indeed exhibits a close representation of the introduced pH filling pattern. The increasing error bar suggests unavoidable mixing occurs within the collection pathway because of the increasing microfluidic pathway to each chamber during the chronological filling process. The various biochemicals are released as a part of sweat components with various release times. The in-vitro study using a dual-valve system displays effective fluid separation and capture in the chambers.

Supplementary material related to this article can be found online at doi:10.1016/j.snb.2023.134441.

2.5. Device feasibility tests

Various biochemicals are excreted through sweat in reaction to stimuli such as physical exertion, cholinergic drug delivery, and environmental effects [50]. The time-dynamic composition and concentration of the excreted sweat from stimulus provide essential information for health monitoring and effective health management. The fabricated device was used to conduct a pilot feasibility human study (SI Fig. 3). This human study quantified the cortisol, lactate, and pH concentrations in sweat, known biomarkers that indicate stress levels, muscle activity, and hydration, respectively [49,60], by evaluating sweat collected by the device during workouts [60]. Subjects engaged in an aerobic and then anaerobic exercise for 15 mins and rested for 15 min at the end of each exercise to yield varying sweat rates and analyte composition. At the end of each exercise were notified for the subjects for accurate transition. The sweat sampling was programmed at 15-minute intervals for each chamber to match the human study program using FHE. The 15-minute intervals were also selected to take into account the physiological lag time of diffusion of sweat analytes from blood to sweat, as well as to collect enough sweat volume for analytical measurement with the designated chamber capacity [1]. The study involves healthy subjects (one male and two females) with dual valve epifluidics with and without TEV activation (Fig. 5A). The fabricated microfluidics were mounted on the arm with FPCB before the human study. The workout time for the subjects was optimized based on the preliminary human studies for a practically relevant range of sweat collection. The on-body human study, as shown in Fig. 5D-K, demonstrates that the sweat information obtained from the non-TEV activated microfluidic device is presented in chronological chamber order, whereas the sweat collection with the TEV activated microfluidic device is timed. Throughout the human study, both non-TEV and TEV activated devices were worn simultaneously. However, the manner of sweat collection in the microfluidic devices distinguishes the quality of the data obtained from each sampling method. This distinction arises from the unknown time of sweat entry into the chambers for the non-TEV activated device, in contrast to the precisely timed collection facilitated by the TEV activated

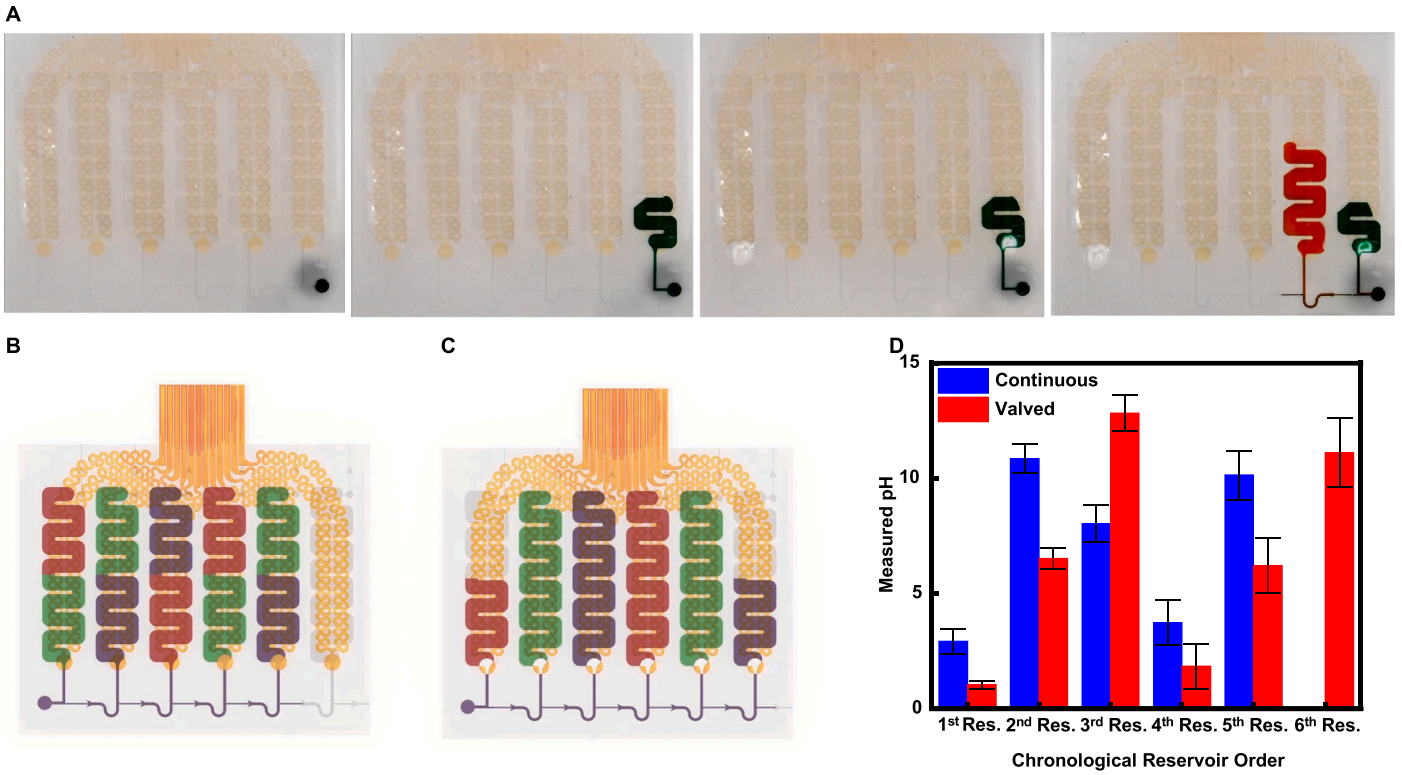

Fig. 4. *In-vitro* testing of microfluidic device with pH solution. A. Sequential image of the TEV mechanism using green and red solution (initial filling of the device using a green solution then a red solution after valve activation). B. Image showing the microfluidic device filling scenario using different pH solution without TEV (Colour indication: Red – pH 1, Green – pH 7, Purple – pH 14). C. Image showing the microfluidic device filling scenario using different pH solution with TEV intervention. D. Measured pH levels of the collected solution from pH filling scenario with and without TEV intervention.

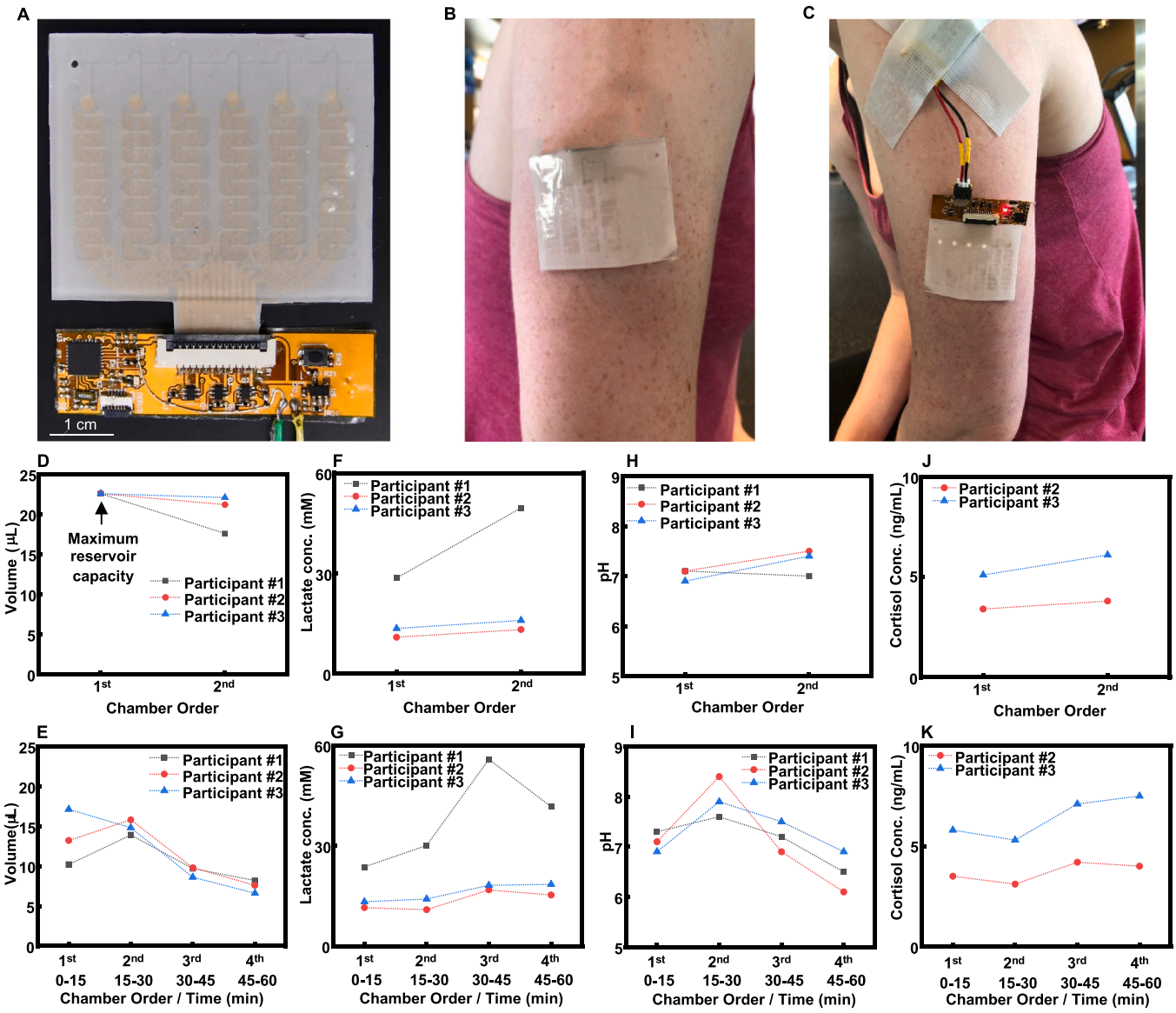

Fig. 5. Human study of the microfluidic device with sweat analysis A. Optical image of the microfluidic device with connected with FHE. B. Optical image of the device with fully collected sweat on the upper forearm without FHE. C. Optical image of the device on the upper forearm with FHE. Graphs showing sweat analyte data from the continuous sweat collection in the chambers without TEV activation for D. sweat volume. F. lactate concentration. H. pH level. and J. cortisol concentration. Graph showing sweat analyte data from timed sweat collection in the chambers with TEV activation for E. sweat volume. G. lactate concentration. I. pH level. and K. cortisol concentration.

device. Sweat volume collected using a dual valve system indicated that the overall sweat rate was higher during the aerobic exercise compared to anaerobic exercise (Fig. 5E). Sweat volume may be used as an indicator of exercise intensity for aerobic and anaerobic workouts. The decrease in sweat volume from aerobic to anaerobic workouts may relate to decreased heart rate, which closely relates to the physiological process from the nature of the workout performed by the human subjects [61,62]. Thus, the sweat volume could not differentiated throughout the human study without the TEV activation (Fig. 5D), which was possible with the TEV (Fig. 5E). The lactate concentration in eccrine sweat increased during the anaerobic workout because of increased muscle fatigue (Fig. 5F-G) [63,64]. The lactate is found in sweat during the human study due to muscle activity through anaerobic respiration. All participants displayed higher lactate concentration during anaerobic exercise than aerobic exercise (Fig. 5F-G). Notably, participant #1, who possesses a muscular physique and engaged in a higher intensity anaerobic workout than the other participants, experienced a significant increase in lactate concentration during the anaerobic exercise. The continuous collection scheme could demonstrate the trend of increasing sweat lactate concentration over the course of workout. However, it does not allow for determining detailed lactate concentrations during the rest periods, which is achievable with TEV-activated devices. Fig. 5H-I show higher pH during the aerobic workout for all participants than the anaerobic workout. The rise in the pH level during aerobic exercise and rest may be attributed to increased sweat volume.

The sweat volume and analyte concentration are closely related, where fewer sweat analytes may be released, or the release of sweat may have overwhelmed the sweat analyte concentration, which may increase the overall pH of the sweat [49,50]. The sweat pH may also have been affected by the intake of fluids or foods before or during the exercise [65]. The pH sweat analysis without TEV activation shows limited information and exhibited average pH from the aerobic and anaerobic workouts because of internal sweat accumulation regardless of the sweat inducement (Fig. 5I). The type of exercise has a minimal effect on sweat cortisol levels (Fig. 5J-K). The release of cortisol in human sweat is associated with various factors and cannot be explained solely by

exercise intensity. However, we observed a minimal increased cortisol concentration during the anaerobic workout session.

The human study verifies the limitations of conventional continuous sweat collection methods, which lack detailed information on changes in sweat composition throughout the study duration. However, the dual-valve system overcomes this limitation by enabling programmed collection of sweat within specific timeframes that correlate with the individual's activities, thereby identifying variations in sweat characteristics. The current device capacity (~168 μL) could hold sweat up to two hours at continuous sweating on the forearm with sweat area opening (0.3175 mm dia.)[18]. The TEV-controlled microfluidics exhibit significant potential in capturing comprehensive changes in sweat composition over time, offering the added benefit of offline measurement capabilities, a feature that may not be available in on-board measurement microfluidic devices.

The future microfluidic device, designed to utilize both onboard and offline measurement of sweat biomarkers during programmed time-based sweat collection, holds particular promise for shedding light on the circadian rhythm of sweat biomarkers, such as cortisol, dehydroepiandrosterone (DHEA), and Neuropeptide Y (NPY), as well as potentially uncovering previously detected or undetected biomarkers. The ability to study these biomarkers in detail will greatly enhance our understanding of their significance and impact, facilitating further advancements in sweat-based diagnostics and personalized healthcare applications.

3. Conclusions

The results demonstrated here to provide an alternative approach to sweat collection for improving the comprehensive knowledge of sweat analytes with time relevancy. The sweat collection device comprises a series of microfluidic chambers with passive and active valve systems. Passive valves enable a controlled microfluidic pathway and the active valves with time-scheduled operation offer isolation of captured sweat in a chamber from the incoming sweat. An in vitro characterization of the device verified the robustness, including reproducibility, the effects of mechanical stresses, microfluidic flow and pressure analysis, and electrical and thermal analysis.

A pilot human study was conducted to simulate the device operation in a real-life application where physical exertion was used as a sweat stimulus. The captured sweat samples with *ex-situ* chemical analysis provided the temporal concentration fluctuation in sweat samples, focusing on the stress biomarker cortisol. The ex-situ analysis capability with state-of-the-art analytical instrumentation can provide vital physiological information about sweat physiology for a wide range of time-dependent sweat biochemicals. To improve the form factor, the chamber size can be adjusted based on the desired volume of sweat to be sampled. Integrating TEV valves within the microchannel layer can also reduce the device thickness and improve its ability to conform to the skin surface. Furthermore, additional components, such as fluid sensors, can be added to redesign the microfluidic device to an automated sweat sampling device. Colorimetric and electrochemical sensing modalities may be integrated with the TEV valves to improve the sweat analyte analysis for real-time and offline measurements synergistically. For long-term liquid storage in the epifluidic devices, a polymer composite such as collagen-PDMS can be used as an alternative. In addition, the results may provide a new study for improving the understanding of the complex human physiology between perspiration, biochemistry, and physiology.

4. Materials and methods

4.1. Microfluidic device fabrication procedure

4.1.1. Channel layer fabrication

A silicon wafer was first deposited with 150 nm of chromium. A positive photoresist (KL5310, KemLab, MA, United States) was spun at 1050 rpm for 45 s and baked at 115 ℃ for 90 s to form a 1 μm thick layer of photoresist on top of chrome deposited silicon wafer. Standard photolithography and development were performed on the silicon wafer to produce a pattern for the wafer. The chrome was etched to leave trenches on the surface of the wafer. The remaining photoresist was removed using isopropyl alcohol and acetone. The remaining Cr on the wafer was used as a passivation layer for deep reactive ion etching creating 200-μm deep channels on the silicon wafer. The remaining Cr was etched, and a thin layer of polymethyl methacrylate (PMMS) (Microchem, MA, United States) was spin-coated on top of the silicon wafer to facilitate the release of the cured PDMS. The silicon wafer produced a channel layer for the final device by pouring PDMS and curing it in a 60 ℃ oven for 6 h.

4.1.2. Elastomeric and expanding layer fabrication

PDMS (10:1 base: curing agent, Sylgard 184, Dow Corning, MI, United States) was spin-coated on a silicon wafer at 4000 rpm for 30 s to form a very thin elastomeric layer for the expanding layer). The PDMS was cured at 60 ℃ for 24 h. Next, PDMS (10:1 base: curing agent) was mixed with Expancel microspheres (031 DU 40, Expancel, Akzo Nobel, Amsterdam, Netherlands) at a 2:1 wt ratio. The mixture was spin-coated on top of the elastomeric layer at 1000 rpm for 60 s and cured at room temperature for 48 h.

4.1.3. Microheater fabrication

The silicon wafer was treated with deionized (DI) water, IPA, and acetone and baked at 150 ℃ for 3 mins. Next, PMMA was spin-coated on the silicon wafer at 1000 rpm for 10 s and then at 3000 rpm for 45 s. The PMMA was cured at 180 °C for 90 s. Polyimide (PI) was spin-coated on top of the PMMA at 1000 rpm for 10 s and then 3000 rpm for 45 s. The wafer was then baked at 90 °C for 3 mins and 120 °C for 3 min. Finally, the wafer was hard-baked at 250 °C for 1 h in a nitrogen gas glove box. The wafer was inserted in an e-beam evaporator to deposit 5 nm of chromium, 800 nm of copper, 5 nm of chromium, and 200 nm of gold over the PI layer. Next, a positive photoresist (KemLab 5310) was spin-coated at 1050 rpm for 30 s and hard-baked for 90 s at 115 °C. A standard photolithography and development process on the wafer produced a pattern for the microheater. Subsequent etching of the gold, chromium, copper, and chromium etchant was used to develop the patterns in the respective layers. The PI layer was created again using the same procedure for the PI encapsulation of the microheaters. Next, the wafer was evaporated with 42 nm of chrome, which acts as the passivation layer during reactive ion etching. The same photolithography and development technique was used to outline the passivation area. Chromium etchant was used to remove unrequired Cr on the wafer. The PI layer was then etched through a reactive ion etching cycle of 90 standard cubic centimeter per minute of O_2 at 300 mTorr for 6 min. The chromium etchant was used again to remove the passivated areas. The microheaters on the wafers were released by soaking the wafer in acetone for 1 h to remove the sacrificial layer of PMMA, and the free-standing sensors were transferred onto water-soluble tape. Finally, 50 nm of silicon dioxide (SiO_2) was deposited through an e-beam deposition for oxygen plasma bonding to the silicon surface.

4.1.4. Final device assembly

Harrick plasma cleaner (PDC-32 G) was used to plasma bond the fabricated layers of the final device. All of the plasma bonding was performed at 500 mTorr, low RF power, 1:4 O_2 to N_2 process gas for 30 s. The SiO_2 deposited microheaters were first plasma bonded with the expanding layer side of the elastomeric layer and the expanding layer. The channel layer was then plasma bonded on the elastomeric side of the elastomeric and expanding layer. Lastly, a thin layer of PDMS was plasma bonded on the side of the expandable layer as a bottom layer. A double-sided medical adhesive was used to attach to the bottom layer of the device for the sweat inlet, with a hole diameter of 0.3175 mm

created using a hole puncher on the adhesive.

4.2. Fabrication of flexible hybrid electronic (FHE)

The lightweight (less than 2.5 g) FHE consists of laser-patterned flexible copper–polyimide–copper printed circuit board (size: 49 mm (L) × 13 mm (W)) populated with commercially available surface-mounted electronic components and FPC/FFC (Flexible Printed Circuit/Flexible Flat Cable) connectors for the programmable power delivery and controlling the microfluidic valves. The FHE contains a low-power microcontroller (STM32L051K8U6, STMicroelectronics, Switzerland), N-channel enhancement mode metal–oxide–semiconductor field-effect transistors (MOSFETs) (2N7002, Diodes Incorporated, TX) for rugged, reliable, and fast switching performance, a linear power regulator, and a serially connected 3.7 V Lipo batteries. The FHE has six MOSFET channels to control the six thermally induced expansion valves (TEVs) on the flexible microfluidic device. The FHE was programmed to activate every 15 min after activation.

4.3. In-vitro measurement of bursting pressure

A pressure-controlled microfluidic delivery system (Fluigent MFCS, Villejuif, France) generated flows for in vitro measurement and analysis of the microfluidic device. In addition, a digital camera was set up on top of the microfluidic device apparatus, filming the microfluidic experiments for flow analysis against time.

4.4. In-vitro TEV experiment using different pH fluid injections

The different levels of pH solutions were individually connected to the fluid divider, M-switch (Fluigent), which allows constant pressurized flow injection of fluid from the connected chambers into the main output channel by selecting the fluid using the accompanied software (SI Fig. 3). The main output channel is connected to the microfluidic device being tested. Injection volumes were estimated by measuring the main channel length to ensure no overfill or less fluid filled in the microfluidic device during fluid change. The constant 1 kPa injection pressure was used to test precise fluid control.

4.5. Image acquisition

Samples of SEM were cut into appropriate sizes to place on the SEM holder using a razor blade then thin layer of Platinum was sputter coated on the surface for SEM imaging. A scanning electron microscope (SEM, S-4800-II, Hitachi, Tokyo, Japan) and a digital microscope (VHX-5000, KEYENCE, Osaka, Japan) produced graphical images of the devices. Nikon's digital camera was also used to capture images of the device for analysis and measurements.

4.6. Mechanical testing

The fabricated devices were tested using a MARK-10 force measurement stand (Model ES-30).

4.7. Human study

The human study protocol was approved by the Institutional Review Board of Binghamton University (STUDY00003072). Written informed consent was obtained from all subjects who participated in the experiments. The designated placement of the device was cleaned with alcohol wipes before device application to minimize any foreign contaminations other than the captured sweat. The FPCB allows precise control of microfluidic valves in the device worn by the participants and is set to activate every 15 min at the start of the human study. The attached microfluidic device was removed from the subjects at the end of the exercise, and sweat collected in each chamber was accessed through a needle incision and collected using a micropipette. The collected sweat from each chamber was analyzed using chemical assay kits for lactate and cortisol purchased from Sigma-Aldrich. pH levels were measured using the Halo Wireless pH Meter with Microbulb from Hanna Instruments Inc.

CRediT authorship contribution statement

Ji Hyun Yang: Conceptualization, Formal Analysis, Data curation, Investigation, Methodology, Validation, Visualization, and Writing – original draft, review, and editing. **Uchekuwu David:** Methodology, Investigation, and Software. **Yeon Sik Noh:** Project administration, Methodology, Supervision, and Writing – review and editing. **Ahyeon Koh:** Conceptualization, Funding acquisition, Project administration, Resources, Supervision, Validation, Visualization, and Writing – review and editing.

Declaration of Competing Interest

The authors declare that they have no known competing financial interests or personal relationships that could have appeared to influence the work reported in this paper. The views and conclusions contained herein are those of the authors and should not be interpreted as necessarily representing the official policies or endorsements, either expressed or implied, of the Air Force Research Laboratory, the U.S. Government, or SEMI-FlexTech. The authors declare that they have no known competing financial interests or personal relationships that could have appeared to influence the work reported in this paper.

Data Availability

Data will be made available on request.

Acknowledgments

This material is based on research sponsored by Air Force Research Laboratory under the agreement number FA8650–18-2–5402. The U.S. government is authorized to reproduce and distribute reprints for government purposes, notwithstanding any copyright notation thereon. This research is also supported by the National Science Foundation (ECCS #1920979), CBET #2238173), and the Small Scale Systems Integration and Packaging (S3IP) Center of Excellence.

Appendix A. Supporting information

Supplementary data associated with this article can be found in the online version at doi:10.1016/j.snb.2023.134441.

References

[1] J.R. Sempionatto, et al., Wearable chemical sensors for biomarker discovery in the omics era, Nat. Rev. Chem. 6 (12) (2022) 899–915.
[2] R. Ghaffari, et al., State of sweat: emerging wearable systems for real-time, noninvasive sweat sensing and analytics, ACS Sens 6 (8) (2021) 2787–2801.
[3] A.J. Aranyosi, et al., Rapid capture and extraction of sweat for regional rate and cytokine composition analysis using a wearable soft microfluidic system, J. Invest Dermatol. 141 (2) (2021) 433–437 e3.
[4] L. Qiao, et al., Advances in sweat wearables: sample extraction, real-time biosensing, and flexible platforms, ACS Appl. Mater. Interfaces 12 (30) (2020) 34337–34361.
[5] C. Legner, et al., Sweat sensing in the smart wearables era: towards integrative, multifunctional and body-compliant perspiration analysis, Sens. Actuators A: Phys. 296 (2019) 200–221.
[6] J. Kim, et al., Wearable biosensors for healthcare monitoring, Nat. Biotechnol. 37 (4) (2019) 389–406.
[7] J. Heikenfeld, et al., Wearable sensors: modalities, challenges, and prospects, Lab Chip 18 (2) (2018) 217–248.
[8] M. Bariya, H.Y.Y. Nyein, A. Javey, Wearable sweat sensors, Nat. Electron. 1 (3) (2018) 160–171.

[9] S. Jo, et al., A review of wearable biosensors for sweat analysis, Biomed. Eng. Lett. 11 (2) (2021) 117–129.
[10] F. Gao, et al., Wearable and flexible electrochemical sensors for sweat analysis: a review, Microsyst. Nanoeng. 9 (1) (2023) 1.
[11] R. Ghaffari, J.A. Rogers, T.R. Ray, Recent progress, challenges, and opportunities for wearable biochemical sensors for sweat analysis, Sens. Actuators B: Chem. 332 (2021), 129447.
[12] T.R. Ray, et al., Soft, skin-interfaced sweat stickers for cystic fibrosis diagnosis and management, Sci. Transl. Med 13 (2021) 587.
[13] A. Koh, et al., A soft, wearable microfluidic device for the capture, storage, and colorimetric sensing of sweat, Sci. Transl. Med. 8 (366) (2016), 366ra165-366ra165.
[14] S. Kim, et al., Soft, skin-interfaced microfluidic systems with integrated immunoassays, fluorometric sensors, and impedance measurement capabilities, Proc. Natl. Acad. Sci. 117 (45) (2020) 27906–27915.
[15] J. Heikenfeld, et al., Accessing analytes in biofluids for peripheral biochemical monitoring, Nat. Biotechnol. 37 (4) (2019) 407–419.
[16] M.C. Brothers, et al., Achievements and challenges for real-time sensing of analytes in sweat within wearable platforms, Acc. Chem. Res 52 (2) (2019) 297–306.
[17] L.B. Baker, Sweating rate and sweat sodium concentration in athletes: a review of methodology and intra/interindividual variability, Sports Med 47 (Suppl 1) (2017) 111–128.
[18] Z. Sonner, et al., The microfluidics of the eccrine sweat gland, including biomarker partitioning, transport, and biosensing implications, Biomicrofluidics 9 (3) (2015), 031301.
[19] Y. Yang, et al., A laser-engraved wearable sensor for sensitive detection of uric acid and tyrosine in sweat, Nat. Biotechnol. 38 (2) (2020) 217–224.
[20] R.M. Torrente-Rodriguez, et al., Investigation of cortisol dynamics in human sweat using a graphene-based wireless mHealth system, Matter 2 (4) (2020) 921–937.
[21] K.C. Lin, S. Muthukumar, S. Prasad, Flex-GO (Flexible graphene oxide) sensor for electrochemical monitoring lactate in low-volume passive perspired human sweat, Talanta 214 (2020), 120810.
[22] Q. Cao, et al., A Smartwatch Integrated with a paper-based microfluidic patch for sweat electrolytes monitoring, Electroanalysis 33 (3) (2020) 643–651.
[23] S.B. Kim, et al., Soft, skin-interfaced microfluidic systems with integrated enzymatic assays for measuring the concentration of ammonia and ethanol in sweat, Lab Chip 20 (1) (2020) 84–92.
[24] L. Wei, et al., In-situ admittance sensing of sweat rate and chloride level in sweat using wearable skin-interfaced microfluidic patch, Sens. Actuators B: Chem. 379 (2023), 133213.
[25] Z. Zhao, et al., A flexible nonenzymatic sweat glucose sensor based on Au nanoflowers coated carbon cloth, Sens. Actuators B: Chem. 388 (2023), 133798.
[26] X. Mei, et al., Wearable molecularly imprinted electrochemical sensor with integrated nanofiber-based microfluidic chip for in situ monitoring of cortisol in sweat, Sens. Actuators B: Chem. 381 (2023), 133451.
[27] L. Fiore, et al., Microfluidic paper-based wearable electrochemical biosensor for reliable cortisol detection in sweat, Sens. Actuators B: Chem. 379 (2023), 133258.
[28] F. Criscuolo, et al., Wearable multifunctional sweat-sensing system for efficient healthcare monitoring, Sens. Actuators B: Chem. 328 (2021), 129017.
[29] H.Y.Y. Nyein, et al., A wearable patch for continuous analysis of thermoregulatory sweat at rest, Nat. Commun. 12 (1) (2021) 1823.
[30] N. Mishra, et al., A soft wearable microfluidic patch with finger-actuated pumps and valves for on-demand, longitudinal, and multianalyte sweat sensing, ACS Sens. 7 (10) (2022) 3169–3180.
[31] J. Xiao, et al., Microfluidic chip-based wearable colorimetric sensor for simple and facile detection of sweat glucose, Anal. Chem. 91 (23) (2019) 14803–14807.
[32] H. Lin, et al., A programmable epidermal microfluidic valving system for wearable biofluid management and contextual biomarker analysis, Nat. Commun. 11 (1) (2020) 4405.
[33] S.B. Kim, et al., Super-absorbent polymer valves and colorimetric chemistries for time-sequenced discrete sampling and chloride analysis of sweat via skin-mounted soft microfluidics, Small 14 (12) (2018), e1703334.
[34] J. Choi, et al., Thin, soft, skin-mounted microfluidic networks with capillary bursting valves for chrono-sampling of sweat, Adv. Health Mater. 6 (5) (2017).
[35] H.B. Lee, et al., A wearable lab-on-a-patch platform with stretchable nanostructured biosensor for non-invasive immunodetection of biomarker in sweat, Biosens. Bioelectron. 156 (2020), 112133.
[36] J.T. Reeder, et al., Waterproof, electronics-enabled, epidermal microfluidic devices for sweat collection, biomarker analysis, and thermography in aquatic settings, Sci. Adv. 5 (1) (2019) eaau6356.
[37] L. Yin, et al., Wearable e-skin microgrid with battery-based, self-regulated bioenergy module for epidermal sweat sensing, Adv. Energy Mater. 13 (4) (2023) 2203418.
[38] L. Manjakkal, et al., Energy Autonomous Sweat-Based Wearable Systems, Adv. Mater. 33 (35) (2021), e2100899.
[39] A.J. Bandodkar, et al., Sweat-activated biocompatible batteries for epidermal electronic and microfluidic systems, Nat. Electron. 3 (9) (2020) 554–562.
[40] A. Alizadeh, et al., A wearable patch for continuous monitoring of sweat electrolytes during exertion, Lab Chip 18 (17) (2018) 2632–2641.
[41] X. Zhu, et al., Nonenzymatic wearable sensor for electrochemical analysis of perspiration glucose, ACS Sens 3 (6) (2018) 1135–1141.
[42] J. Kim, et al., A skin-interfaced, miniaturized microfluidic analysis and delivery system for colorimetric measurements of nutrients in sweat and supply of vitamins through the skin, Adv. Sci. 9 (2) (2022) 2103331.
[43] J. Choi, et al., Soft, skin-integrated multifunctional microfluidic systems for accurate colorimetric analysis of sweat biomarkers and temperature, ACS Sens. 4 (2) (2019) 379–388.
[44] Y. Yu, et al., Proteomic and peptidomic analysis of human sweat with emphasis on proteolysis, J. Proteom. 155 (2017) 40–48.
[45] M.M. Raiszadeh, et al., Proteomic analysis of eccrine sweat: implications for the discovery of schizophrenia biomarker proteins, J. Proteome Res 11 (4) (2012) 2127–2139.
[46] E. Csosz, et al., Highly abundant defense proteins in human sweat as revealed by targeted proteomics and label-free quantification mass spectrometry, J. Eur. Acad. Dermatol. Venereol. 29 (10) (2015) 2024–2031.
[47] C. Liu, et al., The role of sampling in wearable sweat sensors, Talanta 212 (2020), 120801.
[48] H.J. Jang, et al., Electronic cortisol detection using an antibody-embedded polymer coupled to a field-effect transistor, ACS Appl. Mater. Interfaces 10 (19) (2018) 16233–16237.
[49] L.B. Baker, A.S. Wolfe, Physiological mechanisms determining eccrine sweat composition, Eur. J. Appl. Physiol. 120 (4) (2020) 719–752.
[50] L.B. Baker, Physiology of sweat gland function: the roles of sweating and sweat composition in human health, Temp. (Austin) 6 (3) (2019) 211–259.
[51] I.E. Araci, et al., Flow stabilization in wearable microfluidic sensors enables noise suppression, Lab Chip 19 (22) (2019) 3899–3908.
[52] I. Miranda, et al., Properties and applications of PDMS for biomedical engineering: a review, J. Funct. Biomater. 13 (1) (2022) 2.
[53] S. Shin, N. Kim, J.W. Hong, Comparison of surface modification techniques on polydimethylsiloxane to prevent protein adsorption, BioChip J. 12 (2) (2018) 123–127.
[54] B. Heo, et al., A low-cost, composite collagen-PDMS material for extended fluid retention in the skin-interfaced microfluidic devices, Colloid Interface Sci. Commun. 38 (2020), 100301.
[55] Y. Xue, et al., Collapse of microfluidic channels/reservoirs in thin, soft epidermal devices, Extrem. Mech. Lett. 11 (2017) 18–23.
[56] X. Wang, et al., Collapse of liquid-overfilled strain-isolation substrates in wearable electronics, Int. J. Solids Struct. 117 (2017) 137–142.
[57] D.H. Choi, et al., The dynamic response of sweat chloride to changes in exercise load measured by a wearable sweat sensor, Sci. Rep. 10 (1) (2020) 7699.
[58] K. Kwon, et al., An on-skin platform for wireless monitoring of flow rate, cumulative loss and temperature of sweat in real time, Nat. Electron. 4 (4) (2021) 302–312.
[59] C.-H. Wu, et al., Skin-interfaced microfluidic systems with spatially engineered 3D fluidics for sweat capture and analysis, Sci. Adv. 9 (18) (2023) eadg4272.
[60] J. Choi, et al., Skin-interfaced systems for sweat collection and analytics, Sci. Adv. 4 (2) (2018) eaar3921.
[61] M.J. Buono, N.V. Lee, P.W. Miller, The relationship between exercise intensity and the sweat lactate excretion rate, J. Physiol. Sci. 60 (2) (2010) 103–107.
[62] D.-H. Choi, et al., Two distinct types of sweat profile in healthy subjects while exercising at constant power output measured by a wearable sweat sensor, Sci. Rep. 9 (1) (2019).
[63] P.J. Derbyshire, et al., Lactate in human sweat: a critical review of research to the present day, J. Physiol. Sci. 62 (6) (2012) 429–440.
[64] Y. Seki, et al., A novel device for detecting anaerobic threshold using sweat lactate during exercise, Sci. Rep. 11 (1) (2021) 4929.
[65] D. Liu, et al., Wearable microfluidic sweat chip for detection of sweat glucose and ph in long-distance running exercise, Biosens. (Basel) 13 (2) (2023).

Ji Hyun Yang completed his B.E. (Hons) in Chemical and Materials Engineering from the University of Auckland in 2014. He continued his academic journey and obtained an M.E. in Chemical and Biological Engineering from Korea University in 2017. He is a doctoral student in Biomedical Engineering at the State University of New York – Binghamton. His research is focused on developing 3D microfluidic platforms to create intimately integrated interfaces for studying sweat biofluids. He is also, developing innovative biomaterials with a strong focus on biocompatibility, drawing inspiration from bio-inspired and bio-mimetic technologies. Additionally, he is actively investigating methods for sweat capture and collection, aiming to enable noninvasive analysis of biofluids.

Uchekuwu David completed his B.E. in Electrical and Electronics Engineering from Kazaan State Energy University, Russia, from 2016 to 2019. He earned his M.E. in Computer Engineering at the University of Massachusetts Amherst from 2020 to 2022. He is currently a firmware engineer at Apple, specializing in developing low-level firmware for Apple SOCs.

Yeonsik Noh completed his academic journey at Yonsei University, obtaining a B.S., M.S., and Ph.D. in Biomedical Engineering from 2006 to 2013. Following this, he served as a postdoctoral fellow at Worcester Polytechnic Institute from 2013 to 2014, and subsequently at the University of Connecticut from 2014 to 2017. Currently, he holds the position of Assistant Professor in the College of Nursing and the Electrical and Computer Engineering Department at the University of Massachusetts Amherst. Dr. Noh's research focuses on various areas, including wearable biometric devices and circuits, personalized healthcare systems and strategies, the development of health management programs and systems, and underwater health monitoring. He is NSF 2023 career Awardee and has published over 50 papers in esteemed scientific journals and conference proceedings.

Ahyeon Koh holds a B.S. and M.S. in Chemistry from Sogang University, Korea, completing her studies in 2007. In 2013, she earned her Ph.D. in Chemistry from the

University of North Carolina at Chapel Hill. From 2013–2016, she worked as a post-doctoral research associate at the University of Illinois at Urbana Champaign. Dr. Koh is an associate professor in the Biomedical Engineering department at the State University of New York – Binghamton. Dr. Koh's research primarily focuses on interdisciplinary science and engineering approaches, aiming to enhance soft biosensors' chemical and physical biocompatibility. Her work involves utilizing flexible and stretchable platforms to create intimately integrated interfaces. Additionally, she specializes in developing sustainable, bio-inspired, and bio-mimetic biosensing systems. She is one of the pioneers exploring the design of 3D bioanalytical devices for noninvasive biofluid analysis. She has made significant contributions to the field, as demonstrated by her authorship or co-authorship of the papers published in reputable scientific journals and conference proceedings. She is a 2023 NSF CAREER Awardee.